1994

Crystal Structure of an Iodine Phenazine Complex: C12H9N2 + · I3-. C12H8N2 · 1/6I2

Rebecca A. Brandenburg
Iowa State University

Sharon L. Ringrose
Iowa State Universtiy

Robert A. Jacobson
Iowa State University

Let us know how access to this document benefits you

Recommended Citation
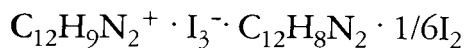
Brandenburg, Rebecca A.; Ringrose, Sharon L.; and Jacobson, Robert A. (1994) "Crystal Structure of an Iodine Phenazine Complex: C12H9N2 + · I3-. C12H8N2 · 1/6I2," *Journal of the Iowa Academy of Science: JIAS, 101(2),*.
Available at: https://scholarworks.uni.edu/jias/vol101/iss2/4

Crystal Structure of an Iodine Phenazine Complex:
$C_{12}H_9N_2^+ \cdot I_3^- \cdot C_{12}H_8N_2 \cdot 1/6 I_2$

REBECCA A. BRANDENBURG, SHARON L. RINGROSE and ROBERT A. JACOBSON

Ames Laboratory and Department of Chemistry, Iowa State University, Ames, Iowa 50011-3020, USA

A structural study of the polyiodide containing species $C_{12}H_9N_2^+ \cdot I_3^- \cdot C_{12}H_8N_2 \cdot 1/6 I_2$ was carried out by single crystal X-ray diffraction techniques. The material crystallizes in the monoclinic space group C2/m with a = 16.561(5), b = 8.372(2), c = 9.908(5) Å and β = 111.24°. There are two molecules per cell. Data were collected using Mo K_α radiation and refinement converged to R = 0.027 based on the 1996 unique reflections with $|F_o| \geq 3\sigma(F_o)$. The iodine atoms were found to exist in two distinct moieties, an I_2 and an I_3^- (symmetric and linear). The iodine-iodine distance are 2.64(1) and 2.917 (1) Å, respectively. The I_2 site is only 1/6 occupied.

INDEX DESCRIPTORS: Triiodide ion, organic iodine complex, phenazine

This study was carried out as part of a series of investigations aimed at structurally characterizing materials which exhibit extended solid state interactions. Of special interest are those species containing mixed oxidation states. Iodine has the ability to form a rich diversity of structures containing iodine in many forms. Our recent study of the structure of dipyridinium decaiodide (T.L. Hendrixson et al., 1991) demonstrated that this structure consists of iodine in the form of the I_3^- and I_7^- anions. This paper reports a structural study of an iodine phenazine complex.

EXPERIMENTAL

Dark red plate-like crystals of the compound $C_{12}H_9N_2^+ \cdot I_3^- \cdot C_{12}H_8N_2 \cdot 1/6 I_2$, were obtained from slow evaporation of a solution containing phenazine and iodine (in excess) in acetone, in the presence of a small amount of hydroiodic acid. An oblong-shaped crystal of approximate dimensions 0.25 X 0.25 X 0.30 mm was used for data collection. Data were collected on a Rigaku AFC6R four-circle diffractometer controlled by a VAX computer with the use of Mo $K\alpha$ radiation (λ = 0.71069Å) and the ω-2θ scan technique. Cell parameters were obtained from a least-squares refinement of 25 reflections in the range 20 < 2θ < 28°. A total of 3307 reflections were collected; after equivalent reflections were merged 1996 unique reflections remained (R_{avg} = 0.033). Of these, 1297 were considered observed reflections with I > 3.00σ (I) and used in all subsequent calculations. The data were corrected for Lorentz and polarization effects, absorption, decay, and secondary extinction.

Table 1. Positional Parameters and B(eq) for $C_{12}H_9N_2^+ \cdot I_3^- \cdot C_{12}H_8N_2 \cdot 1/6 I_2$.

atom	occ	x	y	z	B(eq)
I1		0.0000	0.0000	0.0000	3.41(2)
I2		0.1850(2)	0.0000	0.0518(4)	4.18(2)
I3	0.166	0.0815(3)	0.0000	0.5089(6)	11.3(3)
N1		0.1239(2)	0.6667(3)	0.5404(3)	3.2(1)
C1		0.1991(3)	0.5846(5)	0.2386(4)	4.4(2)
C2		0.1684(2)	0.6668(4)	0.3360(4)	3.8(1)
C3		0.1453(2)	0.5854(4)	0.4416(3)	3.0(1)
C4		0.1031(2)	0.5855(4)	0.6401(3)	2.9(1)
C5		0.0807(2)	0.6679(4)	0.7461(4)	3.7(1)
C6		0.0606(2)	0.5848(5)	0.8454(4)	4.3(2)

Estimated standard deviations in the least significant figure are given in parentheses in this and succeeding tables. Occupancies are unity unless noted otherwise.

STRUCTURE SOLUTION AND REFINEMENT

After a direct methods program failed to give a suitable trial model, a sharpened Patterson map was calculated and starting atomic positions were determined from a weighted Patterson superposition calculated using I(1)-N(1) and I(1)-C(9) vectors. The positions for the H atoms were calculated and not refined. Final refinement with all non-H atoms anistropic converged to R = 0.027 and R_w = 0.032. The quantity minimized was $\Sigma w \, (|F_o| - |F_c|)^2$. The maximum and minimum peaks on the final difference Fourier map corresponded to 0.6 and -0.61 $e^{-}/\text{Å}^3$, respectively. Neutral atom scattering factors were taken from International Tables for X-ray Crystallography and corrected for real and imaginary anomalous dispersion effects (Cromer and Waber, 1974). All calculations were preformed using the TEXSAN (TEXSAN, 1985) crystallographic software package of

Table 2. Selected Intramolecular Bond Distances (Å) for $C_{12}H_9N_2^+ \cdot I_3^- \cdot C_{12}H_8N_2 \cdot 1/6 I_2$.

atom	atom	distance	atom	atom	distance
I1	I2	2.917(1)	C5	C6	1.341(5)
I3	I3**	2.64(1)	C5	C4	1.414(5)
N1	C3	1.342(4)	C6	C6*	1.420(8)
N1	C4	1.343(4)	C1	C1*	1.417(8)
C2	C1	1.345(5)	C3	C3*	1.430(6)
C2	C3	1.413(5)	C4	C4*	1.432(6)

* related by mirror operation
** related by inversion operation

Table 3. Selected Intramolecular Bond Angles (deg) for $C_{12}H_9N_2^+ \cdot I_3^- \cdot C_{12}H_8N_2 \cdot 1/6 I_2$

atom	atom	atom	angle	atom	atom	atom	angle
I2	I1	I2**	180.00	C6*	C6	C5	121.2(2)
C1*	C1	C2	120.8(3)	N1	C3	C2	120.6(3)
C3	N1	C4	119.1(3)	C3*	C3	C2	118.9(3)
C3*	C3	N1	120.5(3)	C1	C2	C3	120.3(3)
N1	C4	C5	120.4(3)	C6	C5	C4	119.6(3)
C4*	C4	N1	120.4(2)	C4*	C4	C5	119.2(3)

* related by mirror operation
** related by inversion operation

Molecular Structure Corporation and the CHES package developed locally. A listing of observed and calculated structure factors is available from the authors.

RESULTS AND DISCUSSION

The crystal structure contains I_2, I_3^-, $C_{12}H_8N_2$ and $C_{12}H_9N_2^+$ moieties. An ORTEP drawing (Johnson, 1976), illustrating the molecular geometries and the atom numbering is given in Fig. 1 while
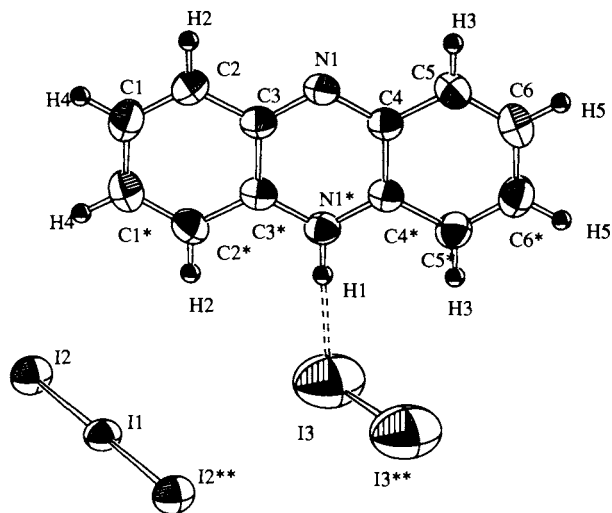

Fig. 1. ORTEP drawing showing the phenazine, I_2 and I_3^- species and their labelling. The thermal ellisoids are drawn at the 50% probability level.

Fig. 2 depicts a PLUTO (Motherwell and Clegg, 1978) drawing of the unit cell. The I_2 site is only partially occupied (~1/6). The distances attained in the I_3^- and the I_2 species agree well with those found earlier in the literature. Literature values for I_3^- range from 2.873 (Dauter et al., 1987) to 3.130Å (Hendrixson et al., 1991) in which the I_3^- distance appears significantly lengthened by interactions with its neighbors; this can be compared to 2.917 Å found in this study. Also, previous reports of the I_3^- species indicate that it can exist in either a linear (symmetric or unsymmetric) or bent form. In our study the I_3^- is symmetric and linear with the central iodine atom residing at a crystallographic inversion center. The distance found for I_2 (2.68 Å) also agrees well with literature values (Mitchell and Cross, 1958). A possible hydrogen bond exists between an iodine
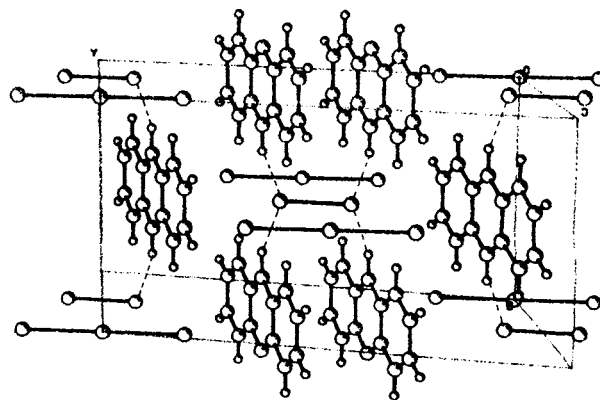

Fig. 2. Unit cell drawing of $C_{12}H_9N_2^+ \cdot I_3^- \cdot C_{12}H_8N_2 \cdot 1/6 I_2$

of the I_2 group and an adjacent nitrogen of the phenazine ring, the iodine-nitrogen distance being 2.87 Å. The phenazine species is planar to within .02Å. The distances in the phenazine group are all within an expected range. The cation and neutral phenazine groups are assumed to randomly occupy the same set of sites in the unit cell. No supercell effects were noticed.

REFERENCES

CROMER, D.T. and J.T. WABER. 1974. "International Tables for X-ray Crystallography", Vol. IV. Tables 2.2 A and 2.3.1.
DAUTER, Z., R. J. MAWBY, C.D., REYNOLDS, D.R. SAUNDERS and L.K. HANSEN. 1987. J. Chem. Soc., Dalton Trans. 1:27-33.
HENDRIXSON, T.L. M.A. ter HORST, and R.A. JACOBSEN. 1991. Acta Crystallogr. C47:2131-2143.
JOHNSON, C.K. 1976. ORTEP II. Report ORNL-5138. Oak Ridge National Laboratory, Oak Ridge, Tennessee.
MITCHELL, A.D. and L.C. CROSS. 1958. "Table of Interatomic Distances and Configuration in Molecule and Ions", Special Publication No. 11 M93.
MOTHERWELL, S. and W. CLEGG. 1978. PLUTO 78. Program for plotting molecular and crystal structures. Univ. of Cambridge, England.
TEXSAN - TEXRAY Structure Analysis Package. 1985. Molecular Structure Corporation.

Failure Analysis of Steel Down-Springs from a John Deere Type 7000 Planter

ADRIA NELSON and L.S. CHUMBLEY

Ames Laboratory, 214 Wilhelm, Ames, IA 50011

Steel down-springs from a John Deere type 7000 Max-Emerge II planter were examined using optical and scanning electron microscopy. The springs in question apply a force to hold the seed-box/planter assembly onto the ground over rough terrain, and they typically suffer from fatigue failure. Springs* under investigation were obtained from two sources, namely, the manufacturer of the planter and a third party vendor. The user of the springs stated that even though the third party vendor springs met manufacturer specifications, they seemed to be failing at a higher rate than the manufacturer's springs. The user requested that the third party springs be examined to determine what, if any, differences existed between them and the springs provided by John Deere, the planter manufacturer. The analysis of the microstructure and the chemical composition revealed the steel used in the springs is of similar composition. However, the amount of inclusions in the third party steel was greater than seen in the John Deere steel, and the quench process to which the third party steel had been subjected appeared to be more severe. The results of this study showed that the difference in purity of the steel, coupled with the difference in quench rate, may have led to an increase in the fatigue failure rate of the third party steel.
*Provided by Mr. Larry Williams, a farmer from Madrid, Iowa

Metal fatigue occurs when a cyclic stress, lower than the yield stress, is applied to a system over an extended period of time. Initiation of a fatigue crack occurs in regions of high stress concentrations, such as notches, microcracks, and impurities. Once nucleated, a crack will slowly propagate with each cycle until the crack length reaches a point of critical fracture and catastrophic failure occurs. Fatigue failure is quite common, particularly in a situation where a large amount of vibrations or cyclic loading is present. This is the case for almost all mechanical devices, which may include a large number of moving parts. This paper will discuss the examination of fatigue failure that occurred in steel springs used on a John Deere type 7000 Max-Emerge II planter. Commonly called down-springs, the purpose of the springs is to apply a load on the planter boxes to hold them on the ground over rough terrain. Thus, they are subject to a cyclic stress state of a large number of cycles. The fatigue failures examined in this study all occurred in springs manufactured by a third party vendor. Similar springs obtained from the planter manufacturer were compared with the third party springs on the basis of microstructure, chemical composition, and hardness.

EXPERIMENTAL PROCEDURE

The springs were examined using optical and scanning electron microscopy (SEM) techniques. The fractures of four third party springs were cut off and optical photographs of the fractures were taken. Two small sections of each spring were also cut off and sliced so that transverse and longitudinal mounts could be made for subsequent hardness testing. Similar samples were made from a John Deere spring. Once mounted, all the samples were ground on SiC grinding wheels, with 80, 240, 320, 400 and 600 grit paper respectively, followed by final polishing using 1 μm diamond paste. The samples were etched with a 5% Nital solution, and low magnification optical micrographs were taken of the samples to determine their macrostructure. Hardness testing was done using a LECO microhardness tester with a load of 1 kg and a dwell time of 15 seconds. A Vickers Diamond Pyramid Hardness reading was taken every tenth of a millimeter across the diameter of each sample in both the transverse and longitudinal directions and the results plotted. The polished samples were examined using the SEM and Energy Dispersive Spectroscopy (EDS) spectra were taken to get a qualitative analysis of the steels' compositions. The fracture surfaces from the third party springs were also examined to determine the initiation points of the fatigue cracks. Finally, slices of both the third party springs and the John Deere spring were examined using an inductively coupled plasma (ICP) to determine the exact composition of each steel.

RESULTS AND DISCUSSION

A fatigue fracture from one of the down-springs is shown in Fig. 1. All of the fractures occurred where the extended cross loop hook [1] of the spring was connected to the body of the spring. The crescent-shaped structure of the crack showed propagation over a period of two years use, as indicated by the varying degree of contrast seen in the fatigue region. Radial cracks pointing back to the initial point of crack initiation could be easily seen (Fig. 2). Low magnification optical and SEM micrographs showed that both the third party and John Deere brand springs had a through-hardened martensitic structure (Fig. 3). However, the third party steel contained a much higher number of inclusions than did the John Deere steel. Such inclusions
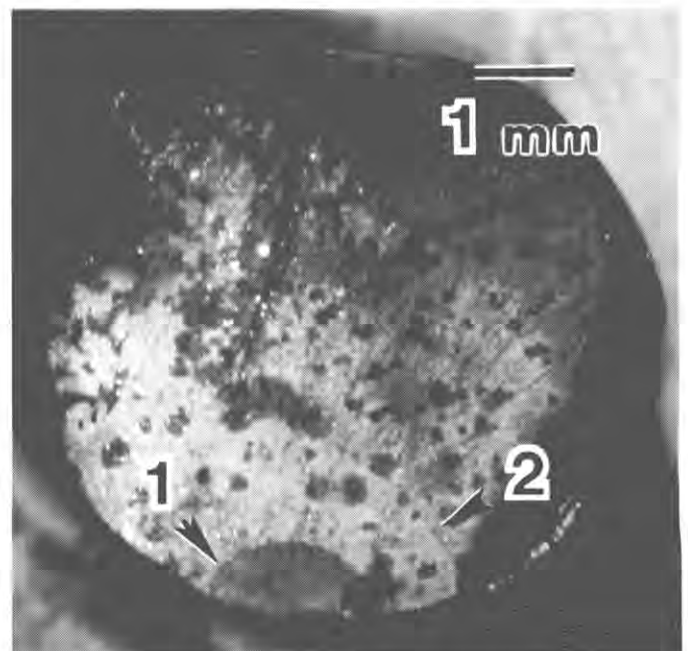

Fig. 1. Low magnification optical micrograph of fatigue fracture showing beach marks. Note the difference in contrast (arrowed as "1" and "2") showing crack propagation over two planting seasons. Dark spots are corrosion products.
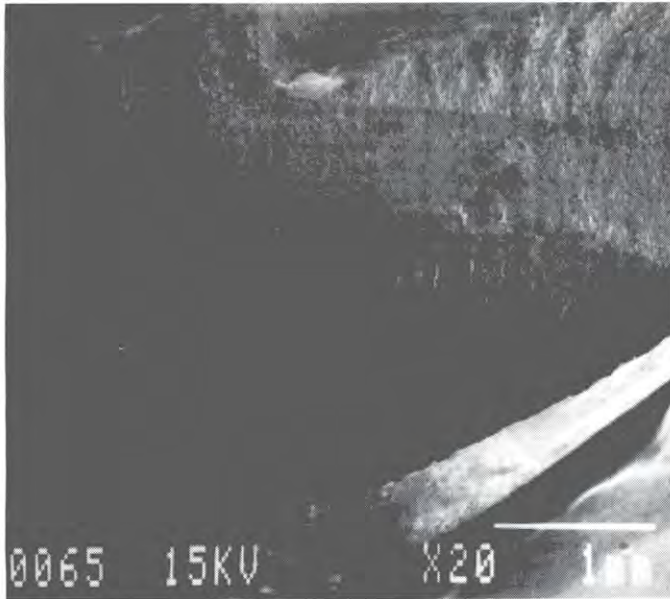
Fig. 2. Low magnification scanning electron micrograph showing beach markings and radial lines emanating from the origin of the crack.

would be expected to decrease the fatigue life of the spring if present on or near the surface of the spring, where they might act as a nucleation site for crack initiation. Close observation of the initiation sites did not reveal any obvious correlation between the initiation points and the inclusions.

The plots of the microhardness, Fig. 4, showed little variation in hardness between the transverse and longitudinal directions due to the drawing process. However, the third party springs were harder on the surface of the coil than in the core, unlike the John Deere spring which had the same hardness all the way through the piece. This would indicate that the third party springs were subject to a more severe quench, such as a water quench, while the even hardness distribution of the John Deere springs is more indicative of an oil quench. This hypothesis is supported by the presence of an internal quench crack in the fracture region of one of the third party spring mounts (Fig. 5) which also suggests a rapid cooling rate.

The EDS scans showed no qualitative difference in Cr, Mn, S or Si composition between the two different springs. Quantitative chemical analysis using ICP showed that the C, Cr, Mn, and S contents of the third party and the John Deere springs are very close, and the results are shown in Table I. The accuracy of the measurements are ± 3%, relative to the numbers shown. Research of the composition and hardness values [2] indicates that the steel used by both manufacturers is most likely an ASTM A229 [3] alloy steel.
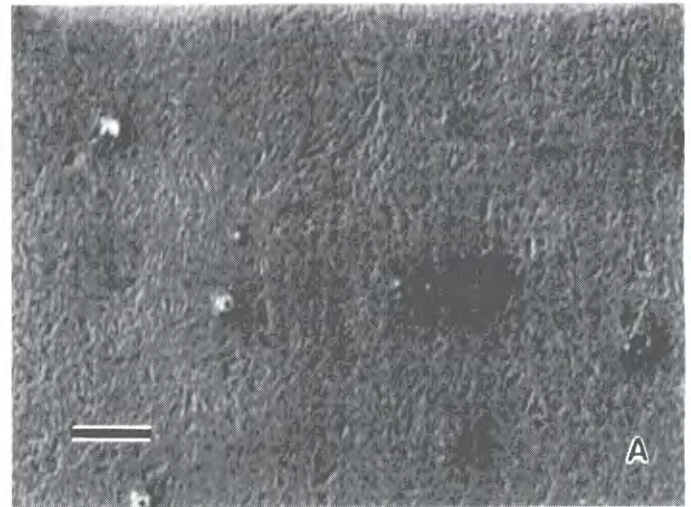

Fig. 3. Scanning electron micrographs showing the martensitic microstructure of the steel used for a) the third party springs and b) the John Deere spring. Note fewer number of inclusions in the John Deere material.

CONCLUSIONS

Although the third party steel contained numerous inclusions compared to the John Deere steel, the EDS results and quantitative chemical analysis indicate that both springs are made from steel specified by ASTM A229. The difference in the microhardness readings of the two springs indicates that the heat treatment of the two springs was different, and the internal quench crack in the third party spring indicates that it was rapidly cooled. Thus, it appears that the John Deere spring was subjected to a slower cooling rate (typical of an oil quench) while the third party manufacturer used a faster water quench. Another possibility is that the John Deere spring was normalized to relieve internal stresses after the spring had been quenched, while the third party manufacturer used the springs in the as-quenched state.

Whether the observed differences predisposes the third party vendor springs to early failure is difficult to say. No direct correlation

Table I: ICP Chemical Analysis - % by Weight

	Third Party Vendor	John Deere
C	0.552	0.567
Cr	0.598	0.613
Mn	0.677	0.703
S	0.010	0.007

Longitudinal Hardness
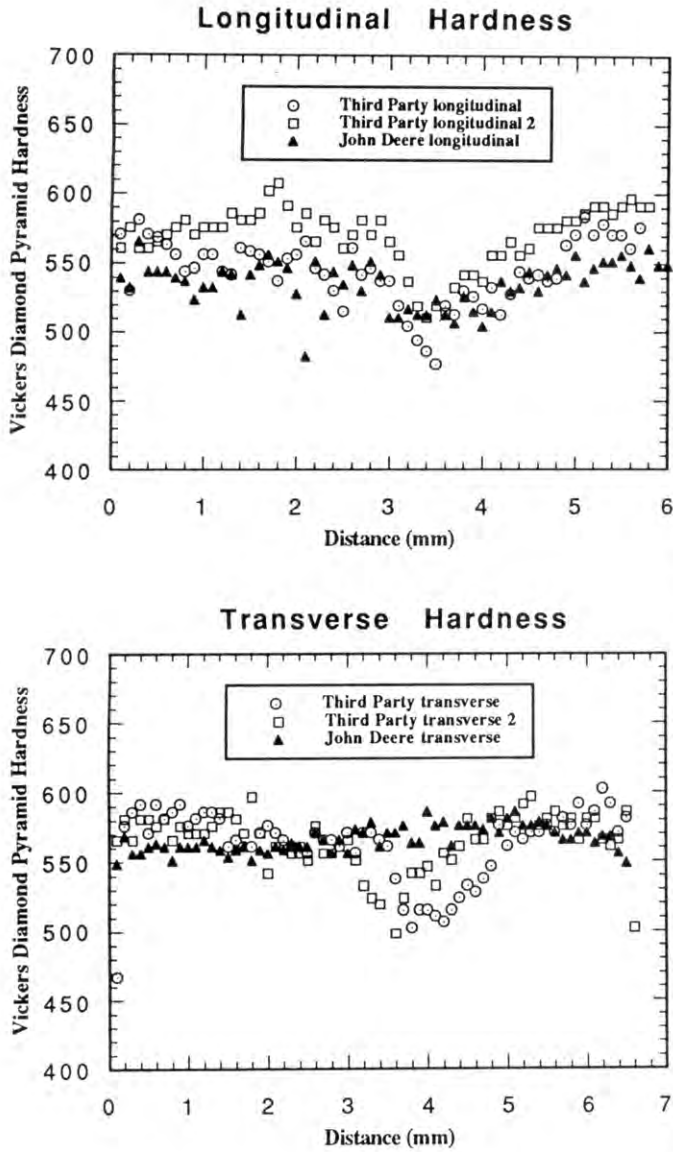

Transverse Hardness

Fig. 4. Plots comparing the microhardness data obtained from two third party springs that fractured to data obtained from a John Deere spring.
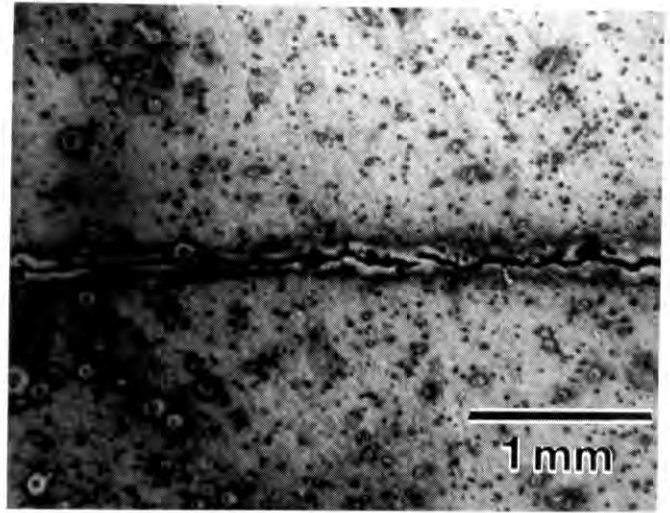

Fig. 5. Low magnification optical micrograph of internal quench crack. The crack did not extend to the edges of the spring. Note staining of the microstructure by the etch around the numerous inclusions.

was seen between the fatigue initiation sites and inclusions or internal cracks in the limited number of springs examined in this study. It can be said with certainty, however, that a clean steel free of internal cracks is a more desirable choice for almost every application.

REFERENCES

1. H. CARLSON, *Springs: Troubleshooting and Failure Analysis*, edited by W.H. Middendorf: Marcel Dekker, New York, 1980.

2. W. MAYERS et. al., *Design and Application of Helical and Spiral Springs-SAE HSJ795*, 1980.

3. B.P. BARDES, Ed., *Metals Handbook Ninth Edition*, 1978, vol. 1, p. 284.

Identifying Sound Radiation from a Discontinuity

PATRICIA DRIESCH

Department of Aerospace Engineering and Engineering Mechanics
Iowa State University, Ames, IA 50011

Every structure has the ability to vibrate. At certain frequencies and conditions, the vibrations can cause sound radiation. This sound radiation is dependent upon the structure's material, shape, and the applied stresses. Although little research has been conducted, discontinuities on structures (i.e. welds, rib attachments, and bolts) have been found to radiate sound and in some cases cause more sound radiation than without the discontinuity. This paper reports work that has identified the significance of unwanted sound radiation, in particular the far-field sound radiation, from two discontinuities. These two discontinuities, a weld and a rib attachment, have very different effects on a structure's properties with mostly local variances. This may be why the two different discontinuities have differing results where the rib attachment displays more significant far-field sound radiation. This paper shows a time domain based method that identifies the variations in wave propagation caused by both a T-shaped rib attachment and a weld added to a beam.

This research is the start of a larger project that has goals of identifying the local variation or combination of variations in a structure that cause the most significant far-field sound radiation. The structures had a discontinuity placed in their middle that were responsible for different variations in the metal. This paper reports the initial results which do not include the specific variations in material, geometry, and residual stresses that are responsible for the sound radiation. The initial results concentrated on the location and significance of the sound radiation caused by the discontinuity itself. The main objectives were to establish standard procedures for the experimental testing and welding, to identify the sound radiation from a weld, and to identify the sound radiation from a rib attachment.

TECHNICAL DISCUSSION

The welding process produces three aberrations in a structure that can cause sound radiation. Welding brings the temperature around the weld past the melting point, which unevenly distributes the temperature throughout the sample. The combination of the phase transformation and nonuniform cooling of the metal's surface and interior cause residual stresses (ASM, 1991, p. 605). Residual tensile and compressive stresses are left in the weldment. Thus, the welding process generates material variances, residual stresses, and geometric variances as possible sources for sound radiation. Testing and procedural techniques that isolate these variables can identify exactly which variation or combination of variations generate the most significant sound radiation.

Thus far, the rib attachment is connected to the beam by screws. As shown in Fig. 1, the T-shaped rib attachment was small in comparison to the beam's length. The rib attachment was fastened by screws holding the two plates to the beam. The connection of the rib attachment to the beam causes residual stresses in the metal near the screws. The geometry of the rib and the disconnection of the material between the rib and the metal may also affect sound radiation. Welded rib attachments will be researched in the future.
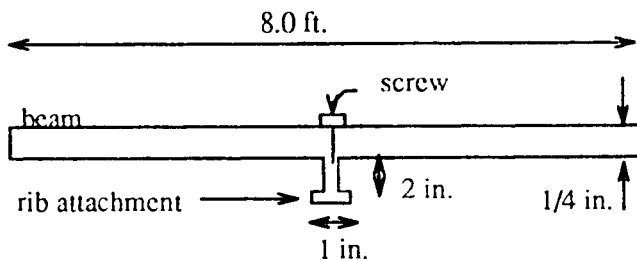
EXPERIMENTAL DESIGN

The experimental design took into account that it must be adjustable to test many different samples with varying dimensions and attachments. To ensure that the design was reliable and yielded valid results, many of the beginning experiments were repeated and checked using both a laster vibrometer and a microphone on samples with and without discontinuities. To limit the environmental sound or background noise, the experimental apparatus was placed in an anechoic chamber. The chamber also eliminates reflections of sound in the measurement area.

The largest part of the design is the baffle, whose purpose is to separate and in turn amplify the sound radiation from the front and back of a sample (Pierce, 1981, p. 213). The baffle is composed of dense particle board with the dimensions 8 feet by 10 feet by ¾ inch (244 x 305 x 1.9 cm). The supports for the baffle allow it to be adjustable in three directions. It can move in one direction at the top and bottom and also move sideways for wider samples (Fig. 2).

Beam samples were used as simplified representations of a structure. Different discontinuities were placed in the middle of each beam (Fig. 1). The ¼ inch (0.64 cm) beam experiments used cold-rolled 1018 steel due to availability, while the ½ inch (1.27 cm) beam experiments used
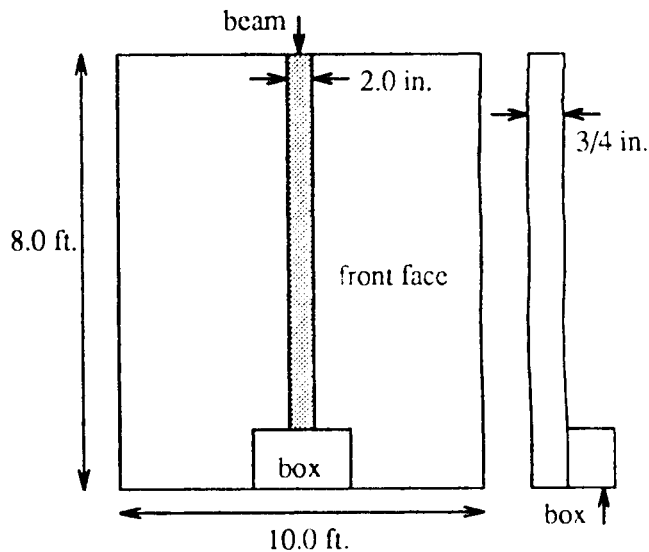

Fig. 1. Geometry and orientation of the rib attachment on the beam.

Fig. 2. Two views of the baffle's design and dimensions.

HY80 steel. The dimensions of the beams were 8 feet by 2 inches by ¼ or ½ inch thick (244 x 5.1 x 0.64 or 1.27 cm).

The bottom end of the beam rested in a bucket of sand, in order to reduce the amplitude of the waves reflected from the bottom of the beam. The top end of the beam was secured to the ceiling for support (Fig. 3).
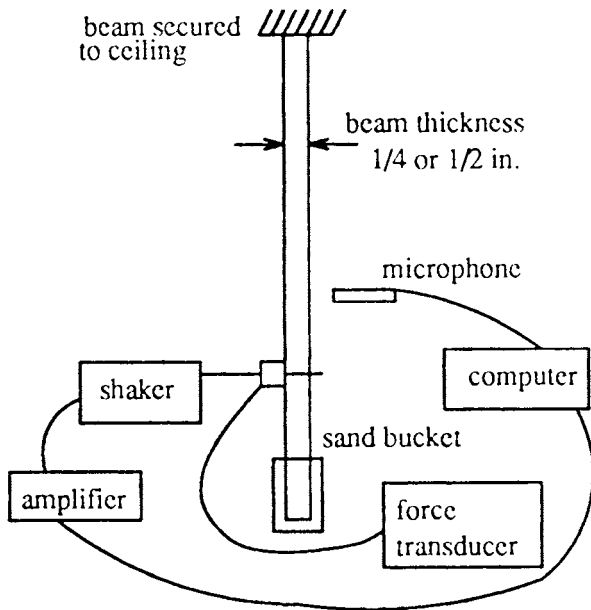

Fig. 3. The general experimental design showing the connections between the shaker, amplifier, force transducer, microphone, and the computer.

A box-shaped structure, also made out of dense particle board, surrounds the sand bucket as an extension of the baffle. Sound damping Fiberglas material was placed inside the box and on top of it for reducing possible reflections off the top of the box and in the bucket of sand (Fig. 2).

EXPERIMENTAL PROCEDURES

The experiments required many procedures for set up along with the actual measurement run itself. A measurement run consisted of measuring the sound pressure or surface velocity at 64 points each located 1 inch (2.5 cm) apart and covered a full range of 63 inches (157.5 cm). Fifteen pressure or velocity signals were averaged at each point. Since the measurement run did not cover the full length of the beam, the locations of the shaker, the discontinuity, and the range of the measurement run were kept consistent in relation to the beam's length for all experiments.

To start the set-up procedures, the baffle was adjusted so that it was aligned flush with the beam's edges without touching the beam, a separation of approximately ¹⁄₁₆ inch. When there were slight variances in the beam and baffle's edges, the beam was kept from touching the baffle anywhere and also from dipping in behind the baffle's front face. The baffle can be adjusted if their are any other variances; for example, thickness, height, width, attachments, and welds. In those cases, edges on welds and attachments must be ground down to be flush with the beam's edges.

The shaker was fastened to the beam between the sixth and seventh measurement point. It was attached by a stinger that protruded through the beam and was secured by a nut. The stinger was then connected to a force transducer (Fig. 3). The location for the hole of the stinger was 20 inches (50 cm) above the bottom of the beam. The first measurement point was 5.5 inches (13.75 cm) below the stinger and the discontinuity was at the thirty-second measurement point.

The measurements using the microphone required three separate set-up procedures. First, the microphone was calibrated by placing it in a pistonphone that has a known sound pressure level. The power supply connected to the microphone was adjusted so that a voltmeter reading the signal from the microphone was 31.7 mV. Second, the robotic scanner was used to move the apparatus holding the microphone to the top measurement and back to the bottom measurement point in order to check that the microphone head was located 0.8 inches (2.0 cm) from the surface of the beam. Third, the signal from the microphone was checked to ensure that background noise from the electrical equipment was insignificant. This could be done by checking that the power cables were not grounded and that all cables were separated. The coherence between the measured signal and the force transducer was checked at a few positions. A value of the coherence of 1.1 to .98 between the force transducer and the microphone's reading indicated that all set up steps were completed properly.

For the data acquisition, the experiment was executed through a computer that: outputs the signal to the shaker, acquires the signals from the microphone and force transducer, moves the scanner holding the microphone to each of the 64 points, and then stores the signals from the microphone and force transducer. The experiments were run for the two frequency ranges of 500-2000 Hz and 2000-4000 Hz.

Another procedure that was established to prepare the beams with their discontinuities was the welding process. The welding process was a gas metal-arc (commonly called MIG) process (Sacks, 1976, p. 289-328). For each weld, the voltage range of the welding machine was medium (30-39V), arc voltage was 6V, and the wire speed was 6 ipm. The ¼ inch beams had a single-V butt weld and the ½ inch beams had a double-V butt weld with a 45° angle for both types of welds (Sacks, 1976, p. 821). The beams were clamped to the welding table during both welding and cooling to keep them from warping. See Fig. 4 for an example.
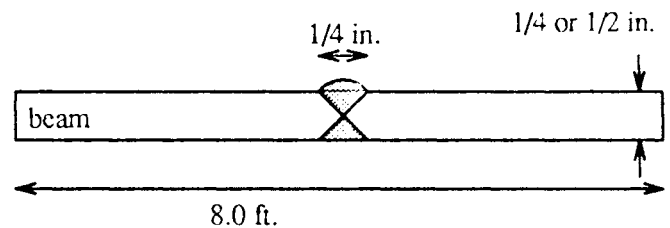

Fig. 4. Geometry and dimensions of the double-V butt weld on a beam.

DATA PROCESSING

Refer to Fig. 5 as the data processing is described. Experimental data, the files containing the signals and their appropriate locations on the measurement run, were transferred to the Project Vincent DECstation Computer System where two main data processing files were created. The first file was directly used to store time data created by using our designed filter and response forces. A desirable bandpass filter has a steep square-like frequency filter that only allows a designated frequency range into the file when used. A desirable force response has a sharp peak with small to no secondary peaks (Wilson, 1989, p. 113). A force response was designed to simulate a force that did not interfere with the wave propagation being observed. Design of this force was discussed by Mann and Williams (1992) and Kruger (1992).
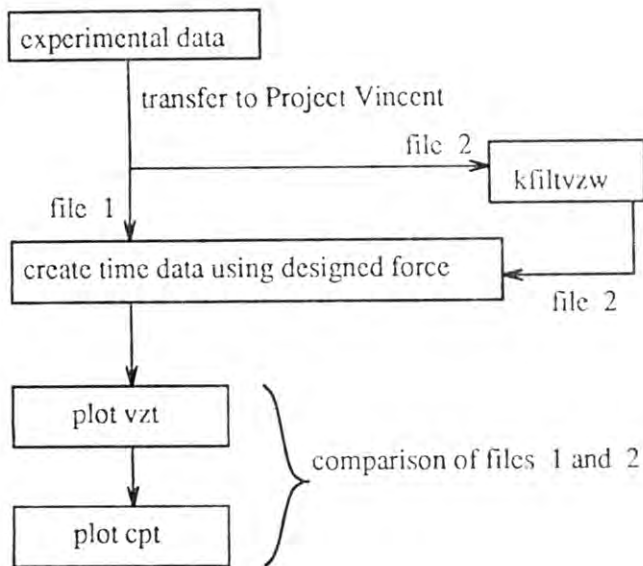
Fig. 5. An outline of the data processing.

The first file's data were then plotted as time versus position, a vzt graph, as shown in Fig. 6. The horizontal position on the graph refers to the positions on the measurement run, where point A is the first measurement point. The waves propagate, to the right, away from the shaker, located at point B, where the waves are reflected from the rib
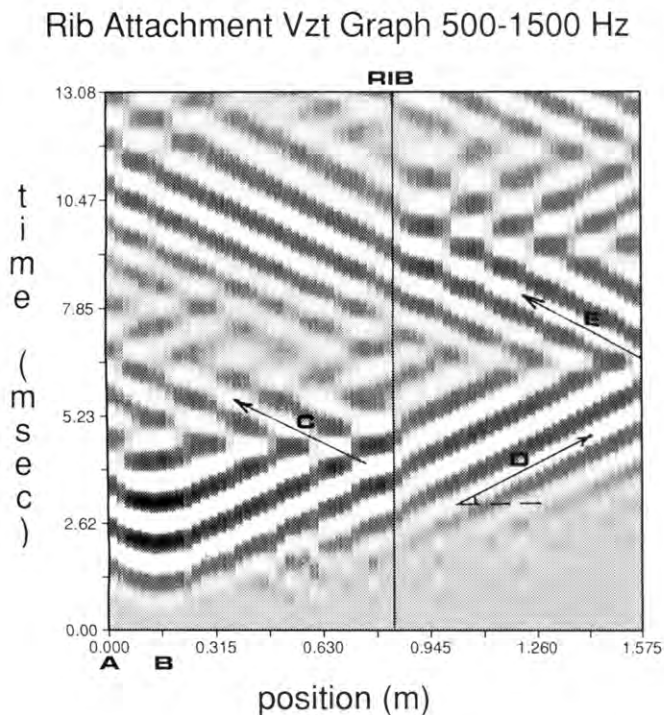

Fig. 6. Vzt plot of wave propagation: beam with rib attached to the beam. A: first measurement point; B: location of shaker; C: waves reflected from rib; D: waves propagating past rib; E: waves reflected from support at the top of the beam.

attachment, point C. The waves that continue through the discontinuity are marked with a D. The waves then continue to reflect off the ends of the beam and discontinuity until it becomes difficult to identify the paths of propagation. For this reason, analysis of the graphs concentrated on the initital reflections.

The phase speed (m/s) is represented by the angle between the horizontal and the wave. The graphs compare position (m) and time (s), where the inverse of the slope (s/m) is the phase speed (m/s). Mann and Williams (1992) describe this data processing procedure. The data were also used to plot a cpt graph. Cpt graphs show the time versus phase speed for a single measurement position. See Fig. 7 for an example. The cpt graph uses a grey scale where the darker color represents a larger phase speed.
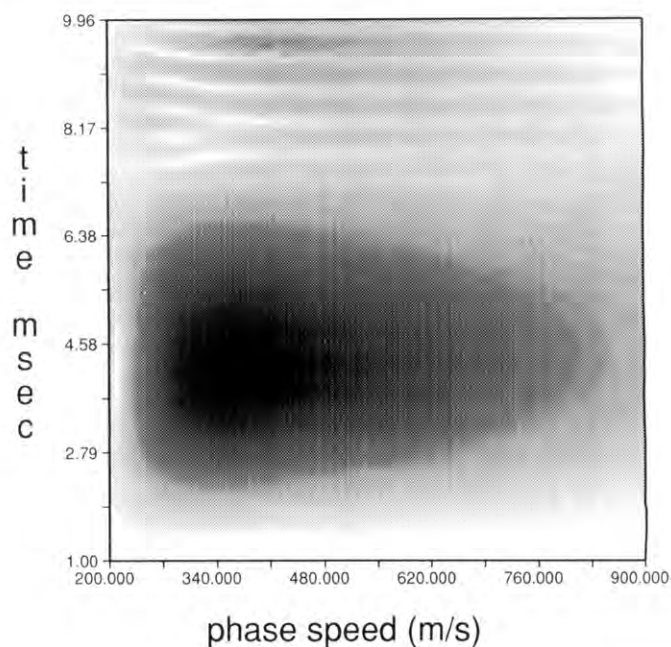

Fig. 7. The phase speed of the welded beam at the weld. Dark represents high amplitudes.

The original data were also sent to a program that separated far-field sound radiation from near-field sound radiation. The near-field sound radiation is the sound heard up close to a source, and eventually dies out with distance away from the beam. The far-field sound radiation is responsible for the detection of vibrating structures miles away. For this project, the far-field sound radiation was of more interest. After the near-field sound radiation was filtered out, the data followed the same data processing as described for the first file. The two sets of graphs were then compared and analyzed. In more detail, Fig. 8 is Fig. 6 after the near-field sound radiation was filtered out, leaving the far-field sound radiation represented on the graph. Point A is the first measurement point while point B is the shaker which displays a high concentration of far-field radiation as would be expected. The significance of the far-field sound radiation is represented by the more intense and distinguishable waves at that position on the graph. Therefore C represents a high concentration of far-field sound radiation at that location.

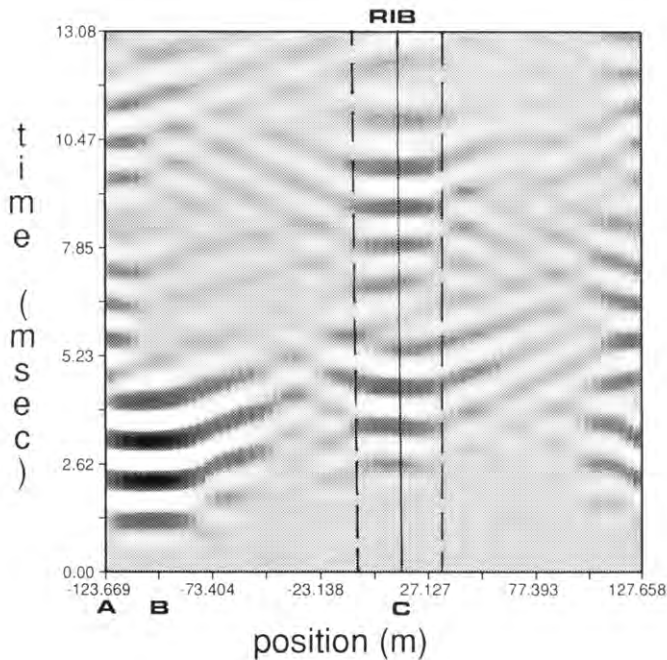## Rib Attachment Kfiltvzw Vzt Graph 500-1500 Hz

Fig. 8. The distribution of far-field sound radiation in reference to time and position along the beam. A: first measurement point; B: shaker location; C: location of rib.

from the discontinuity. The angle increase of the wave propagation immediately after the rib attachment demonstrates that the phase speed is decreased by the attachment. These observatons are seen in Fig. 6. The cpt graph in Fig. 7 displays the peak incident phase speed at the weld (point 32) which is slower than 413-418 m/s, the average phase speeds for the ¼-inch samples. The vzt and cpt graphs in Figures 6 and 7 were before the near-field sound radiation was filtered out. The vzt graph in Fig. 8, after removing the near-field sound radiation, displayed the far-field sound radiation. There is a high concentration of far-field sound radiation at the rib attachment.

(5) The welded ½-inch experiments do not display any apparent wave reflections of far-field sound radiation from the weld. See Fig. 9.

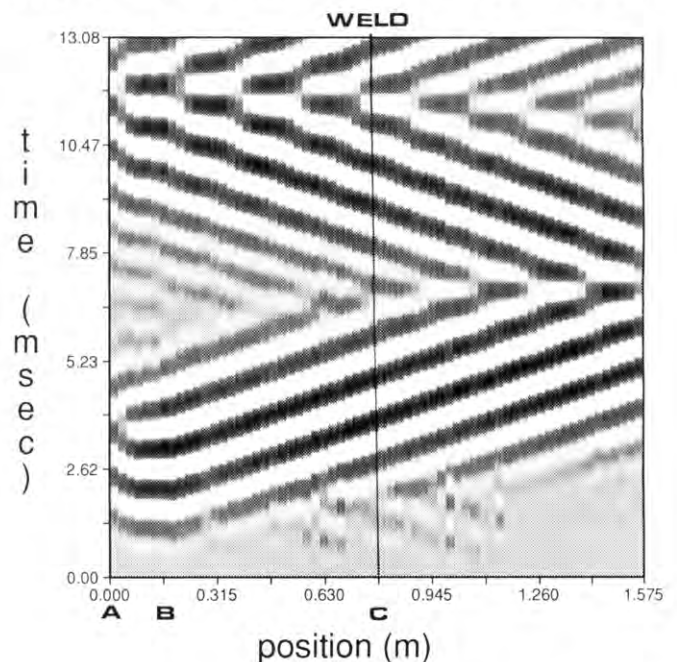## Welded Microphone Vzt Graph 500-1500 Hz

Fig. 9. Vzt plot of wave propagation: beam with weld. A: first measurement point; B: shaker location; C: location of weld.

RESULTS

In an attempt to establish a standard measurement procedure, many repetitive experiments were run in search of defects and errors. After precautionary steps were taken, the experimental design and testing procedures were reliable, repeatable, and valid.

The welding process was established after one change was made. The beams needed to be clamped to a rigid surface, otherwise significant warping would occur. The welding process itself formed a weldment with the three properties typical of welds, (1) the beams warp due to residual stresses, (2) a rough half cylindrical shaped weld, and (3) discoloration due to material variances. Through observation, the three properties are much more distinct in the ½-inch (1.27 cm) samples.

Through data processing and analysis, some initial results were obtained for the identification of the sound radiation from the discontinuities.

(1) For the data processing, the bandpass filter and force responses were designed, balancing the desirable and undesirable qualities. Through experimentation, the force's time interval could be no longer than 2.6 msec, otherwise the different waves plotted as time data were indistinguishable.

(2) A result established early on in the experimentation is that the welded, unwelded, and microphone experiments for the ¼-inch samples displayed no differences between them, including comparisons at different frequencies. Thus the microphone will be used in all future measurements, because it is easier to use than the laser vibrometer.

(3) The ½-inch samples showed faster propagation speeds of 426-454 m/s compared to 413-418 m/s for the ¼-inch samples, although they still propagated through the beam in the same time interval.

(4) From the rib attachment's vzt graph, there are reflections observed

CONCLUSIONS

From the ¼-inch experiments with the weld, one conclusion can be made. The ¼-inch welds are smaller than the ½-inch welds and the experiments show no differences before and after welding. It would be more productive for any further experiments concerning welds to be conducted on the ½-inch or thicker beams.

Some conclusions can be made at this point about the rib attachment. It does reflect and locally change the wave propagation, with a high concentration of far-field sound radiaton around the rib attachment. This would lead one to assume the rib is responsible for significant far-field sound radiaton. At this point, though, we do not know what variation of the discontinuity is responsible for these results.

Identifying the variations responsible for the sound radiation from the rib attachment or the weld would require many more experiments. The rib attachment has apparent effects on the sound radiation, but techniques need to be developed in order to identify the specific causes of sound radiation. The variations possibly responsible are the vari-

ances in geometry, variances in the applied stresses from the attachment, or the discontinuity of the material between the rib and the beam. In contrast, the geometry variance of the weld is smaller than with the rib attachment. The variances are more internal, such as the material and residual stress changes, so they may require different data processing techniques.

A consideration for easier analysis is to use lower frequencies. At lower frequencies, the waves' phase speed is slower, making the interactions between the waves more distinguishable.

Another consideration for easier analysis is to replace the sand bucket with a different damping fixture to hold the beam. The vzt graphs show that there are still some reflections off the sand, which complicate the vzt graphs. The reasonsing for using the sand bucket was to dampen the waves, leaivng only the initial waves traveling to the right on the vzt graphs. Reducing the reflections from the sand would simplify and clarify the path of propagation.

Overall, this preliminary research has established some standard procedures to follow and the initial results display areas that need refining and further research. This research has also indicated where the future research should concentrate.

ACKNOWLEDGEMENTS

REFERENCES

AMERICAN SOCIETY FOR METALS INTERNATIONAL. 1991. *American Society for Metals Handbook: Vol. 4 Heat Treating.* American Society for Metals International.

KRUGER, DANIEL H. 1992. "Radiated Sound Energy of a Point-Driven, Fluid-Loaded, Cylindrical, Spherically End-Capped Shell as a Function of Force Time Duration and Multiple Pulse Spacing." M.S. Thesis, Iowa State University.

MANN III, J. ADIN, and E.G. WILLIAMS. March 4-6, 1992. "Determining the Amplitude of Propagating Waves as a Function of Phase Speed and Arrival Time," Proc. Second International Congress on Recent Developments in Air- and Structure- Bourne Sound and Vibration, Auburn University.

PIERCE, A.D. 1981. *Acoustics, an Introduction to its Physical Principles and Applications.* New York: McGraw Hill.

SACKS, RAYMOND. 1976. *Welding: Principles and Practices.* Peoria: Chas. A. Bennett Co.

WILSON, CHARLES E. 1989. *Noise Control.* New York: Harper & Row.